PAPER

Investigation of molten metal droplet deposition and solidification for 3D printing techniques

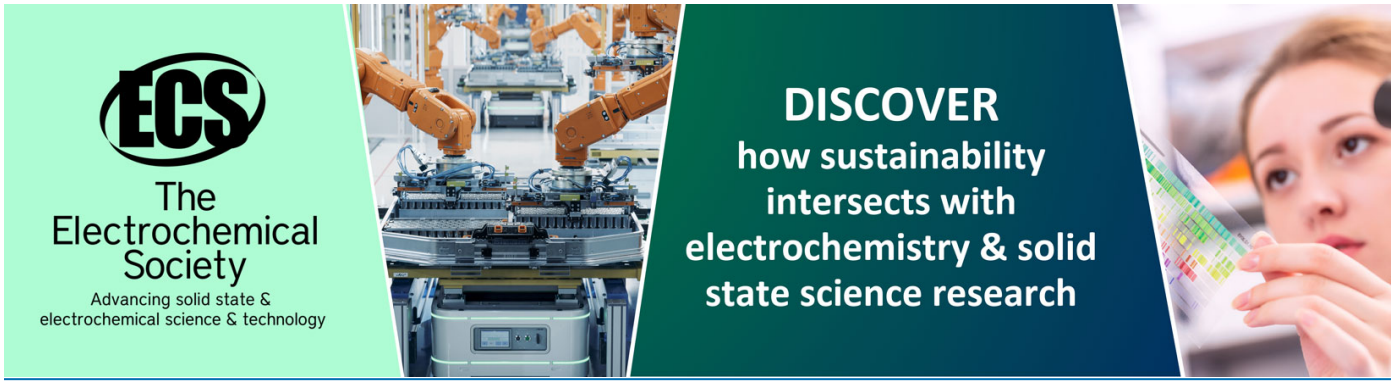

IOP Publishing Journal of Micromechanics and Microengineering
J. Micromech. Microeng. **26** (2016) 095012 (14pp) doi:10.1088/0960-1317/26/9/095012

Investigation of molten metal droplet deposition and solidification for 3D printing techniques

Chien-Hsun Wang, Ho-Lin Tsai, Yu-Che Wu and Weng-Sing Hwang

Department of Materials Science and Engineering, Research Center for Energy Technology and Strategy, National Cheng-Kung University, No.1, Ta-Hsueh Road, Tainan City 70101, Taiwan

E-mail: wshwang@mail.ncku.edu.tw

Received 5 January 2016, revised 27 April 2016
Accepted for publication 3 May 2016
Published 8 July 2016

Abstract

This study investigated the transient transport phenomenon during the pile up of molten lead-free solder via the inkjet printing method. With regard to the droplet impact velocity, the distance from nozzle to substrate can be controlled by using the pulse voltage and distance control apparatus. A high-speed digital camera was used to record the solder impact and examine the accuracy of the pile up. These impact conditions correspond to We = 2.1–15.1 and Oh = 5.4×10^{-3}–3.8×10^{-3}. The effects of impact velocity and relative distance between two types of molten droplets on the shape of the impact mode are examined. The results show that the optimal parameters of the distance from nozzle to substrate and the spreading factor in this experiment are 0.5 mm and 1.33. The diameter, volume and velocity of the inkjet solder droplet are around 37–65 μm, 25–144 picoliters, and 2.0–3.7 m s^{-1}, respectively. The vertical and inclined column structures of molten lead-free solder can be fabricated using piezoelectric ink-jet printing systems. The end-shapes of the 3D micro structure have been found to be dependent upon the distance from nozzle to substrate and the impact velocity of the molten lead-free solder droplet.

Keywords: lead-free solder, inkjet printing, pile up, micro droplet, solidification

(Some figures may appear in colour only in the online journal)

1. Introduction

Inkjet printing technology using molten metal droplets for deposition and solidification has drawn considerable attention in academic research and for its practical applications [1–6]. However, the limitations of ink printability have restrained its use with regard to some new technologies, such as the pile up of inkjet printing for 3D structures, wafer-level packaging concept fabrication, and the production of sensor functional materials for micro-electro-mechanical systems (MEMS) packaging [7–9].

Over the last few years, inkjet printing technology has made great improvements in print quality and reproduction speed, and is now widely used in the modern electronics packaging industry [10–12]. This approach has proven to be a highly successful non-contact printing process and form of micro-pattern fabrication, with lead-free solders being used in a wide range of printing applications. The merits of this approach include variable drop size, high precision in positioning, rapid prototyping, and low production cost. However, parameter adjustment is necessary when operating a piezoelectric device at high temperature in order to pile up the molten metallic droplets in stable formations. Therefore, an understanding of how the jet height and pulse voltage variations are influenced by the process conditions is essential for successful ink-jet printing in this context.

Although a large number of studies have been made of inkjet printing, little is known about the physical phenomena related to the pile up of bump shapes and droplet spreading. Tsai *et al* [13] examined the effects of the pulse waveform on droplet formation behavior in a series of experimental tests. Their results showed that molten lead-free solder can be jetted

in multiple droplets, a main droplet with satellites, and single droplets. Son *et al* [14] discussed the effects of the shapes and positions of the droplets when using the droplet jetting method, with these two factors corresponding to a function of the height. An increase in jet height lead to a decrease in surface ripples, and thus droplets with a smooth surface. The height variations were more than 2.3 mm, and the positioning accuracy of the jetted solder droplets decreased rapidly as the jet height increased. Tian *et al* [15] examined solidification in relation to solder bump formation in a solder jet process, and simulations were also applied using volume of fluid (VOF) models to examine solder droplets impinging onto fluxed and non-fluxed substrates. Based on these results, complete rebound occurs during the process of the solder droplet impinging onto the fluxed substrate, and a cone-shaped solder bump forms onto the non-fluxed substrate. Attinger *et al* [16] demonstrated a method of molten micro-droplet surface deposition and solidification using solder jetting technology. The transient behavior of the spreading and solidification processes highlights the importance of two features with regard to spreading after the molten micro-droplets impact the flat substrate, and these are oscillations and freezing. Haferl and Poulikakos [3] proposed that the impact velocities of the molten droplets affect the final shapes of the observed pile up structures. Schiaffino *et al* [17] examined the spreading of droplets that occurs in a short period, where the flow is driven by the dynamic pressure of impact and resisted primarily by inertia, as shown in earlier research into molten droplet deposition and solidification on a solid substrate. The impact process of the molten solder droplet can be subdivided into four phases. First, there is the initial impact phase (pre-impact), in which the droplet hits the substrate. In the second phase (spreading), the spreading of the droplet is driven by the dynamic pressure of impact over time. In the third phase, the droplet comes to post-spreading oscillations in a process of recoil followed by inertial oscillations. In the fourth phase, the droplet comes to solidification [17, 18]. Haferl *et al* [19] simulated the transport and solidification phenomena of molten droplet (63%Sn–37%Pb solder) on a substrate. The columnar structures were piled up by micro-droplets with a low Weber number and formed a recirculation zone due to an instantaneous vortex formed in the vicinity of the contact line. Li *et al* [20] simulated the successive deposition of molten Al droplets on a horizontally moving substrate by a volume of fluid (VOF) method and experimental validation, and the molten Al droplets simultaneously solidified through heat transfer to the substrate. Chao *et al* [21] studied the remelting and bonding of deposited aluminum alloy droplets under different droplet and substrate temperatures. The experiment results showed that the good remelting and metallurgical bonding between droplets were determined by a suitable combination of droplets temperature (700 °C) and substrate temperature (450 °C). Zuo *et al* [22] observed the non-isothermal deposition behavior of molten aluminum droplets for 3D printing technology, and found that the local solidification and interfacial re-melting phenomena play an important role in the first spreading/recoil cycle.

However, to date little is known about how the ejected droplets impact the surface of the substrate, and thus there is still a lack of basic understanding about this, such as the dynamic behavior of the pile ups that occur between droplets. Shin *et al* [23] examined the jetting behavior of liquids with various viscosities and surface tensions. The results showed that the impact and pile up of droplets are influenced by the surface tension (σ), viscosity (η), and density (ρ) of the fluid. The relative magnitudes of surface tension, viscosity, and inertial forces are analyzed by the Reynolds number (Re) and the Weber number (We). Based on the non-dimensionalization scheme outlined above, the Weber (We), Reynolds numbers (Re) and Ohnesorge number (Oh) are defined as follows [3, 16, 4, 24, 25–28]

$$\mathrm{We} = \frac{\rho D_0 \nu^2}{\sigma}, \tag{1}$$

$$\mathrm{Re} = \frac{\rho D_0 \nu}{\eta}, \tag{2}$$

$$\mathrm{Oh} = \frac{\eta}{\sqrt{D_0 \sigma \rho}}, \tag{3}$$

where ν is the impact velocity of the droplet, ρ and σ are the density and surface tension of the droplet, respectively, η is the droplet's dynamic viscosity, and D_0 is the initial diameter before impact.

This paper aims to investigate the behavior of ejected molten droplets under different process parameters, from their impact on the substrate to the occurrence of pile up. Deposition experiments were performed to analyze the appropriate forming conditions for achieving successive pile up of molten droplets by the drop-on-demand (DOD) inkjet printing method, which will provide a fundamental understanding of the role of the pile up in the molten solder jet process. The effects of the jet height and variations in impact velocity of successive droplets on the deposit shapes of the pile up were recorded. It is anticipated that the results can help provide a useful method to achieve the appropriate pile up of solder formation under high temperature conditions for the fabrication of micro structures.

2. Experimental methods

2.1. Apparatus and method description

In order to investigate transient pile up during the process of inkjet printing, an observation system was established between the nozzle and the substrate as part of the droplet impact experiment. The method described in this article for pile up drop formation and drop impaction on a gold-plating glass surface is based on a high-speed digital camera system (HSDC), and utilizes the setup shown schematically in figure 1. This figure shows a solder jet apparatus for four interlocking functional blocks, namely the pneumatic, heating, printing and monitoring blocks. The pneumatic block used nitrogen to alter the back-pressure of the solder reservoir, and this served

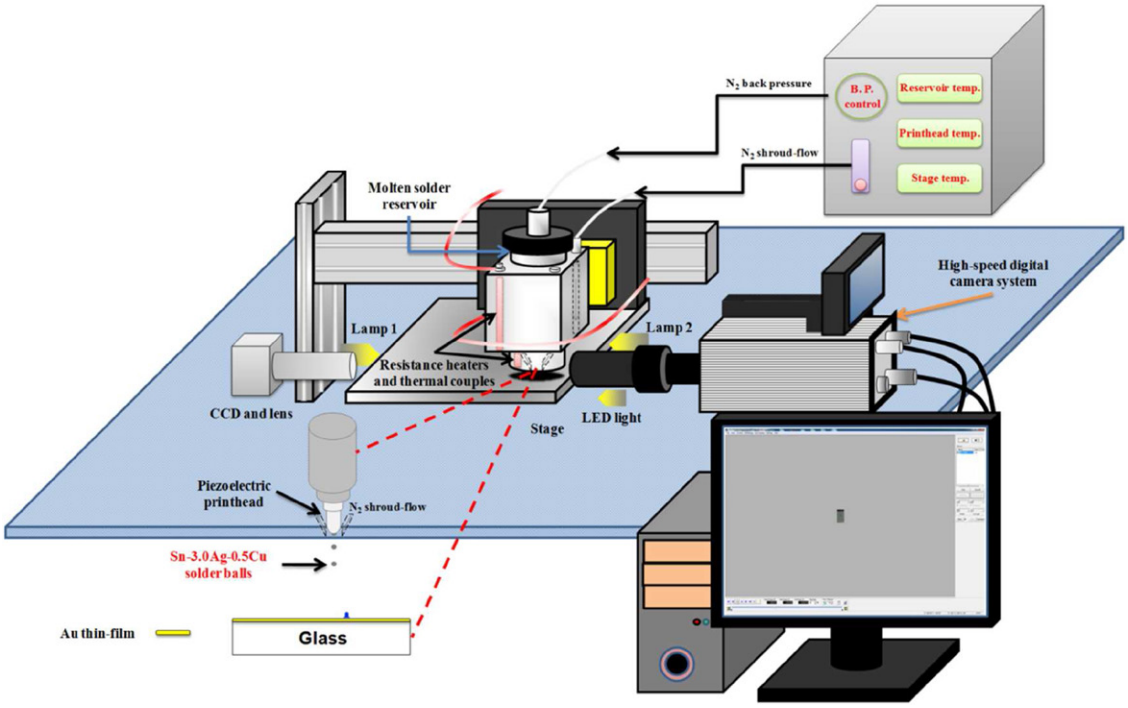

Figure 1. Schematic diagrams of the experimental apparatus for the molten metal and high-speed digital camera system.

Table 1. The initial conditions of the inkjet printing system.

Condition	Pulse time (μs)					Frequency (Hz)	Pulse voltage (V)			Jet height (mm)	Reservoir pressure (kPa)
	T_{rise}	T_{dwell}	T_{fall}	T_{echo}	$T_{finalrise}$		V_{DC}	V_1	V_2		
A	30	10	5	10	5	400	−40	−35	−45	0.5–5	6.8
B	30	10	5	10	5	400	−40	−35	−50	0.5	6.8
C	30	10	5	10	5	400	−40	−35	−55	0.5–5	6.8

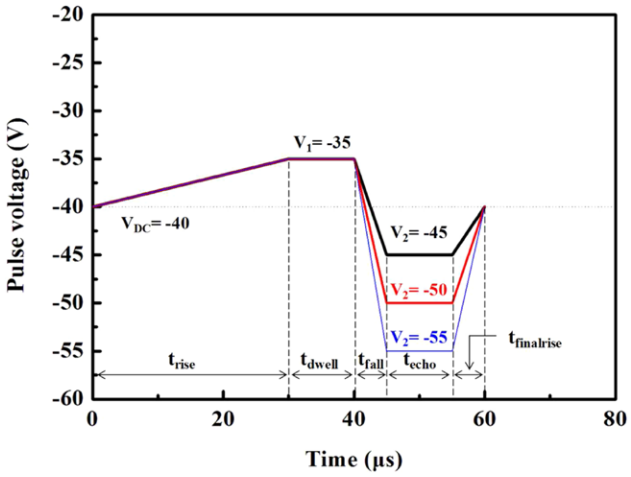

Figure 2. A schematic diagram of the bipolar waveform conditions.

as a curtain around the path of the droplet toward the nozzle, limiting interaction with the circumjacent air. The heating block enabled the solder to melt in an enclosed reservoir, and could maintain a temperature of up to 230 °C with resistance heating. The printing block consisted of a piezoelectric print head to enable a solder jetting driver that is pressurized to shape droplets using a bipolar waveform of varying pulse time and voltage. A piezoelectric print head (MJ-SF-04-50-8MX, MicroFab Technologies Inc.) is employed as a dispenser head with a 50 μm diameter orifice, fixed on the Z axis. The monitoring block was used to observe and record the pile up of droplets, and included a charge-coupled device (CCD) camera with a microscope objective lens and a light emitting diode (LED). The delay in time between droplet generation and the moment the picture of each droplet was taken was gradually increased. This method will be here referred to as flash videography, and requires good repeatability both in time and position of the generated droplet. When a stable single droplet was emitted, the camera system was triggered and captured images of the transient droplet. In addition, the present study used a high-speed digital camera (HSDC) system to record the physical changes and phenomena that occur when the droplets impact the substrate surface and pile up the solder at a high frequency (up to 198 000 fps). Images of the final pile up shapes were obtained with a good resolution using a high-speed camera (Memrecam GX-3, NAC Image Technology) system. Two halogen lamps faced the nozzle and the camera lens. Lamp 1 was used as the background light, and lamp 2 was located on the side of the high-speed digital camera lens to improve the droplet contour from the nozzle to the lens. When the high-speed digital camera display shows a cross-section,

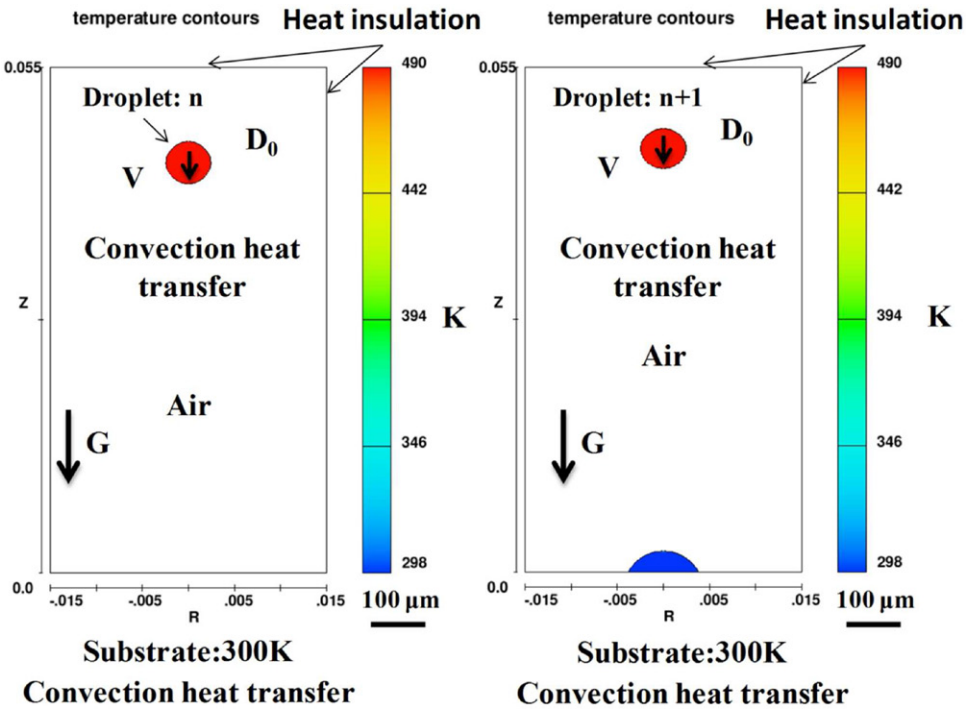

Figure 3. Schematic of the numerical model for molten metal droplet deposition.

Table 2. Thermal and physical properties of Sn–3Ag–0.5Cu used in the numerical simulations.

Parameters	Value	Unit	Symbol
Density	7500	$kg \cdot m^{-3}$	ρ
Viscosity	2	$mPa \cdot s$	μ
Surface tension coefficient	0.431	$N \cdot m^{-1}$	σ
Liquidus temperature	221	°C	θ_l
Solidus temperature	216	°C	θ_s
Thermal conductivity of liquid	73	$W \cdot m^{-1} \cdot °C^{-1}$	k_{pl}
Specific heat of liquid	250	$J \cdot kg^{-1} \cdot °C^{-1}$	C_{pl}
Latent heat of fusion	67 762	$J \cdot kg^{-1}$	L
Contact angle	60	°	θ
Deposition distance	0.5, 2, 5	Mm	D

the optical axis of the high-speed digital camera is horizontal to the substrate. Some parameters of the control system were modified to capture the shape of the droplet pile up, such as frame rate, frame size and shutter speed.

The morphology was observed by scanning electron microscopy (SEM, JEOL JSM-7001F). The SEM images were all taken at 10 KV, 600× magnifications. Energy dispersive x-ray (EDX) was also used to determine the elemental composition at selected areas.

2.2. Materials and sample preparation (molten lead-free solder)

A commercial Sn–3.0Ag–0.5Cu lead-free solder was used as the ink material. Sn–3.0Ag–0.5Cu ternary eutectic solder has a melting temperature of ~217 °C. Substrates were prepared via sputtering (40 mA, 600 s) from a gold target. The Au thin films were then placed in a chamber under a vacuum (20 Torr) at room temperature. The thicknesses of the Au thin films were found to be 208 nm using SEM.

2.3. Inkjet printing conditions

The inkjet printing conditions were used to produce molten droplets on demand. Table 1 summarizes the variables of the printing conditions with regard to the bipolar waveform and reservoir back-pressure. Figure 2 shows a schematic diagram of bipolar waveform conditions. The bipolar waveform was set to be 30 μs for T_{rise}, 10 μs for T_{dwell}, 5 μs for T_{fall}, 10 μs for T_{echo}, and 5 μs for $T_{finalrise}$. The pulse voltages were set as V_1 of −35 V, V_{DC} of −40 V and V_2 of −45 to −55 V, where the negative voltages were used to overcome the electronic issues of the piezoelectric print head, based on Tsai *et al*'s [13] and Son's *et al*'s [14] findings. In the inkjet printing process, the molten metal solder fills a reservoir and must be pressurized by nitrogen. For a Sn–3.0Ag–0.5Cu solder jet, an appropriate nitrogen shroud-flow near the orifice of the print head was pumped at 2.5 L min^{-1}, which was 6.8 kPa of the back-pressure in the reservoir. The protecting gas (nitrogen) surrounding the piezoelectric print head allowed the fluent refill of the capillary and avoided oxidation.

2.4. Numerical model

Following the work of Hirt *et al* [29], the volume of fluid (VOF) method was used with a fractional value of F to provide a simple and fast way to track free boundaries. The volume fraction of each fluid is tracked through the state. For $F = 1$, the mesh cell is entirely filled with liquid. While for $F = 0$, it is empty (dispersed phase). When the mesh cell instantaneously contains a part of the interface, both phases coexist

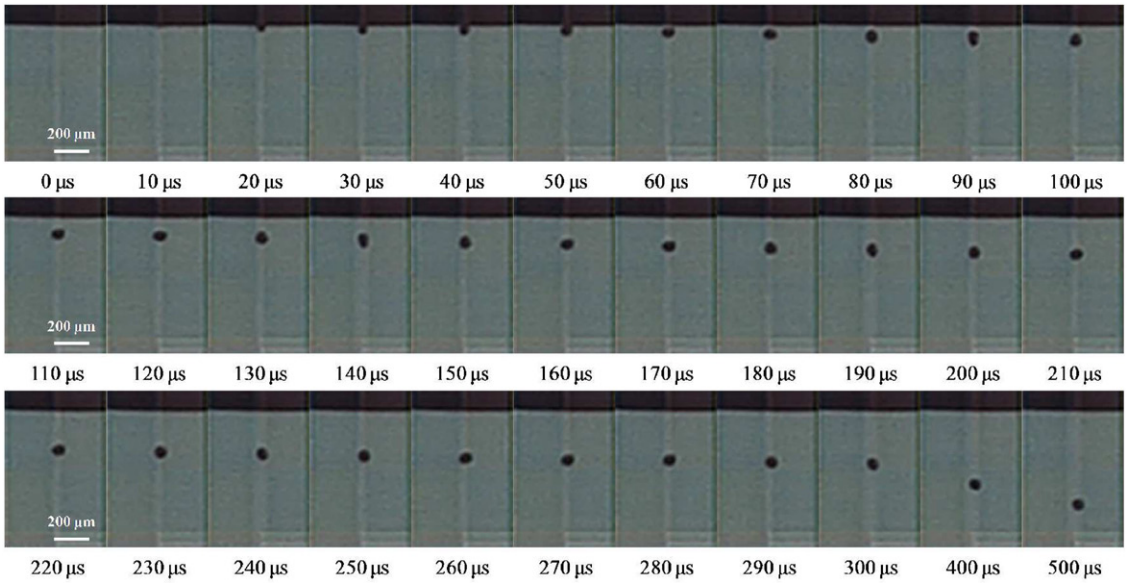

Figure 4. Temporal evolution of droplet formation for Sn–3Ag–0.5Cu solder with condition B ($T_{\text{rise}} = 30$ μs, $T_{\text{dwell}} = 10$ μs, $T_{\text{fall}} = 5$ μs, $T_{\text{echo}} = 10$ μs, $T_{\text{final}} = 5$ μs, $V_1 = -35$ V and $V_2 = -50$ V) in table 1.

and it is $0 < F < 1$. The time dependence of F is described by the equation:

$$\frac{\partial F}{\partial t} + \frac{1}{V_F}\left[\frac{\partial}{\partial x}(FA_x u) + \frac{\partial}{\partial y}(FA_y v) + \frac{\partial}{\partial z}(FA_z w)\right] = 0, \qquad (4)$$

where u, v, and w are the velocity components in Cartesian coordinate directions (x, y, z). A_x, A_y and A_z are the fractional area of fluid flow in the x, y and z directions, respectively.

The initial conditions of the numerical model for molten metal droplet deposition are shown in figure 3. The computational domain of the two-droplet pileup can be observed in the substrate and droplet. The impact velocities of the droplets produced by inkjet printing are utilized in the results of this study. A grid size of 2 μm × 2 μm was applied for an axisymmetric uniform mesh of 20 625 elements in cylindrical coordinates. The interfacial temperature of the wall of the substrate was set at 300 K. v is the impact velocity of the molten droplet, D_0 is the diameter of the molten droplet, and there is a convective heat transfer boundary condition at the wall, while convective heat transfer occurs from air to droplet. Therefore, the fluid mechanics and heat transfer involved in the pileup process are considered in the model as the initial free surface shape and the boundary conditions, respectively [19]. From a general point of view, the molten droplet pile up in metal microdroplet deposition is influenced by droplet size, speed, liquid surface tension, temperature and substrate properties. In order to validate the numerical model, the simulated pileup used a commercial code, Flow 3D Version 11.0.4 (Flow Science, Inc, Santa Fe, NM, USA), as an aid to analyze the molten metal droplet pileup in an impact process. With regard to the simulation process conditions, the thermal and physical properties of Sn–3Ag–0.5Cu that were used are shown in table 2, and listed as follows: density $\rho = 7500\,\text{kg} \cdot \text{m}^{-3}$, viscosity $\mu = 2$ mPa · s, surface tension coefficient $\sigma = 0.431\,\text{N} \cdot \text{m}^{-1}$, thermal conductivity of liquid $k_{pl} = 73\,\text{W} \cdot \text{m}^{-1} \cdot {}^{\circ}\text{C}^{-1}$, specific heat of liquid $C_{pl} = 250\,\text{J} \cdot \text{kg}^{-1} \cdot {}^{\circ}\text{C}^{-1}$, liquidus temperature of solder $\theta_l = 221$ °C, solidus temperature of solder $\theta_s = 216$ °C and latent heat of fusion $L = 67\,762\,\text{J} \cdot \text{kg}^{-1}$. These conditions were taken from a number of earlier studies [13, 15, 30], while the substrate temperature was 300 K. The molten metal droplet deposition process can be divided into the spreading and the post-spreading oscillations, and the present work mainly focuses on the pile up of droplets.

3. Results and discussion

3.1. Sequential molten solder droplet pile up

Figure 4 shows the single droplet formation processes of Sn–3Ag–0.5Cu solder with condition B ($T_{\text{rise}} = 30$, $T_{\text{dwell}} = 10$, $T_{\text{fall}} = 5$, $T_{\text{echo}} = 10$, $T_{\text{finalrise}} = 5$ μs, $V_1 = -35$ V, $V_{\text{DC}} = -40$ V, $V_2 = -50$ V and jet height = 0.5 mm) in table 1. In the period of 0–50 μs, the droplet was pushed outward. At 60 μs, the droplet was completely detached from the nozzle. Meanwhile, a spherical droplet with a diameter of 48 μm and a 3.5 m s^{-1} impact velocity was formed, which then impacted the substrate from 60 μs to 500 μs.

The evolution of droplet impact onto a gold-plated substrate was recorded using high-speed digital camera with condition B in table 1, as shown in figure 5(a). Figure 5(a) shows continuous frames of a solder droplet impacting on the substrate. In this experiment, the pre-impact diameter and the impact velocity of the metal droplet were 48 μm and 3.5 m s^{-1}, respectively. The distance between the nozzle tip and substrate surface was 0.5 mm. Because the above parameters were used, therefore the Reynolds number Re = 627.0, Weber number We = 9.0, Ohnesorge number Oh = 4.8×10^{-3}. The droplet of fluid was nearly stable, and the shape appeared to be spherical before impact. It was observed that the first droplet spread out to its maximum diameter of about 63.0 μm along the surface of the substrate from 0 μs to 10 μs. In this

phase, the spreading of the droplet is driven by the dynamic pressure of impact over time. Mundo *et al* [31] reported that droplet splashing occurs with a Weber number in the range of 100–1000. Thoroddsen *et al* [32] investigated the fingering pattern of an impacting drop, and found that when fingers were observed at the edge, the Reynolds number and the Weber number were equal to 15 000 and 1000, respectively. The droplet recoiled back to the highest point in the vertical direction and its movement was resisted by inertia at 20 μs. Here the molten solder was in the pre-solidification phase between the droplet and substrate. From 20 μs to 200 μs the droplet starts post-spreading oscillations in a process of recoil followed by inertial oscillations. Finally, the equilibrium stage of the droplet is reached at 350 μs. Figure 5(b) shows an SEM image of the droplet deposited on the gold surface. The image in figure 5(b) is of a droplet that has completely solidified after impacting on the gold-plated substrate.

Figure 6(a) show 2D images of the temperature contour of a single droplet impacting on the gold-plated substrate at 490 K with an impact velocity of 3.5 m s^{-1}. The numeral symbol represents the number of recoil times. At 10 μs, the molten droplet spread on the substrate. The spreading of the molten droplet is caused by the impact velocity. At 20 μs, the first recoil was observed, and then the droplet comes to the highest point in a process of rebound, instantaneously. This phenomenon formed 4 times between 20 and 350 μs. The possible reason was related to the inertial oscillations during the post-spreading oscillations of the droplet. Finally, the droplet reached its static state at 350 μs. The results show that the molten droplet has been stuck to the substrate. It means that heat transfer of the molten solder simultaneously cooled to the substrate. The underdamping of the oscillations is connected to the viscous dissipation. Figure 6(b) shows the simulated deformation and solid fraction of a 48 μm diameter Sn–3Ag–0.5Cu solder droplet on the gold-plated substrate at 490 K with an impact velocity of 3.5 m s^{-1}. The colors of the scale bar represent with the same variation of solidification contours from red to blue as followed descriptions. It was found that the first droplet spread out to its maximum diameter of about 75 μm along the surface of the substrate from 0 μs to 10 μs. At 20 μs, it was observed that the phenomenon of solidification initiated occurred on the bottom of the molten droplet. The range of solidification increases when the time increases from 20 to 350 μs. The numerical simulation was validated based on the results of this experiment, as obtained with the high-speed digital camera system. It follows from what has already been said that there are four times the number of post-spreading oscillations. In this phase the droplet starts to solidify, which is initiated from 20 μs to 350 μs. The numerical simulation for this phase makes it clear that the temperature (490 K) of the liquid below the molten droplet decreased. There are two phases in the solidification that occur within 350 μs. There is an early phase (figure 6(b)), in which solidification is initiated at 20 μs, and then a later phase with complete solidification at 350 μs, which is comparable to what was observed in the experiments (figure 5(a)). In addition, a comparison of the numerical simulations and experimental findings shows that

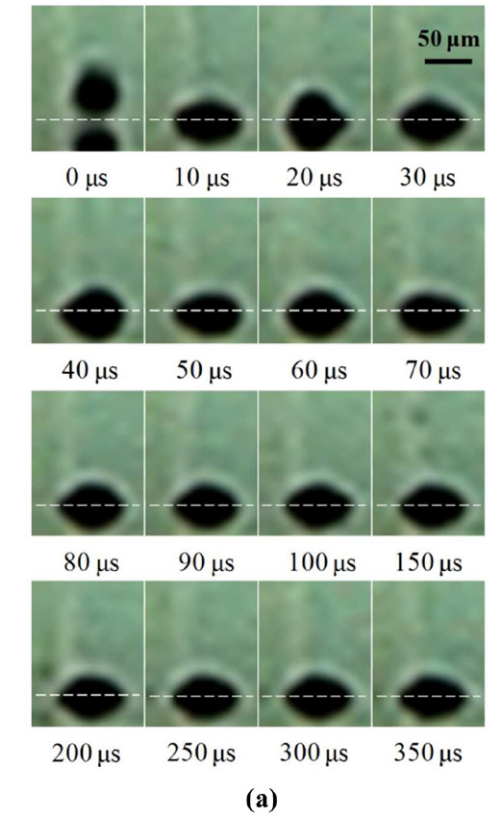

Figure 5. (a) Evolution of droplet impact onto a gold-plated substrate recorded using a high-speed digital camera with condition B in table 1. The distance from a jet nozzle to a substrate is 0.5 mm. The dashed lines demarcate the line of droplet impact on the substrate, which separate the outline of the droplet from that of its reflection on the substrate. (b) Tilted 40° SEM image of the droplet deposited on a gold-plated substrate.

the heights of the deposited droplets were 21 μm and 24 μm, respectively. Rapid spreading is followed by underdamped interfacial oscillations with a longer timescale (from 20 μs to 200 μs) than seen with the spreading (from 0 μs to 10 μs). Under limited recoil the oscillation was observed to stop after about 200 μs, and when the four spreading and post-spreading oscillation processes had been completed. Finally, observation of the post-deposition final shape shows that the first droplet was completely solidified and appeared to be oval at 350 μs.

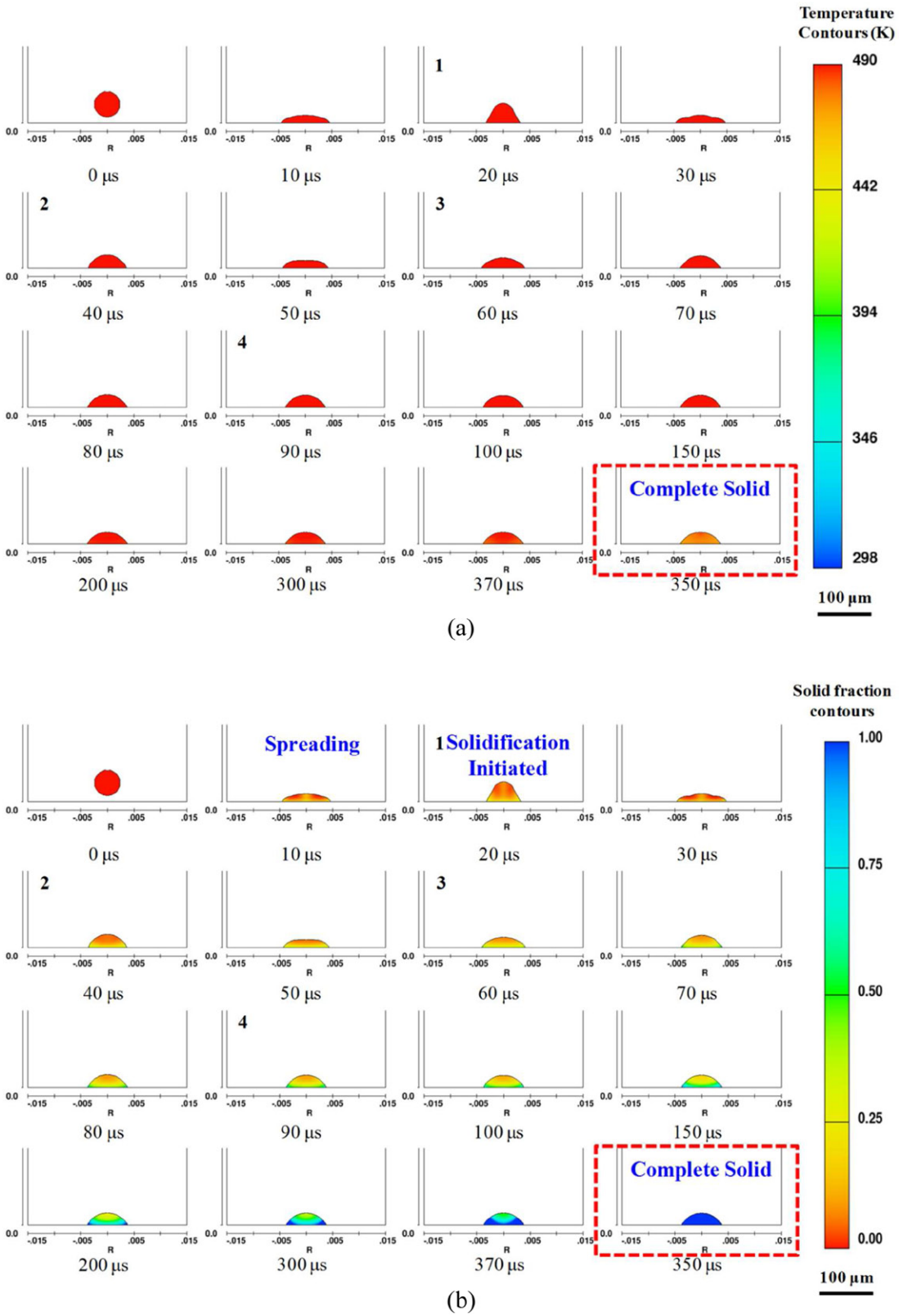

Figure 6. (a) Calculated 2D images of the temperature contour of a single droplet. (b) Simulated deformation and solid fraction of a 48 μm diameter Sn–3Ag–0.5Cu solder droplet on the gold-plated substrate at 490 K with an impact velocity of 3.5 m s^{-1}. The numeral symbol represents the number of recoil times.

Figure 7(a) shows the evolution of the droplet impact and solder pile up process for experimental observations with condition B in table 1. The second droplet is deposited on top of a solidified droplet of the same material, and the distance from the jet nozzle to the substrate is 0.5 mm. The second (molten) droplet impacts on the first (solidified) droplet at 10 μs and then slightly spreads on the solidified droplet. Afterward, the second droplet continues to recoil and oscillate until the

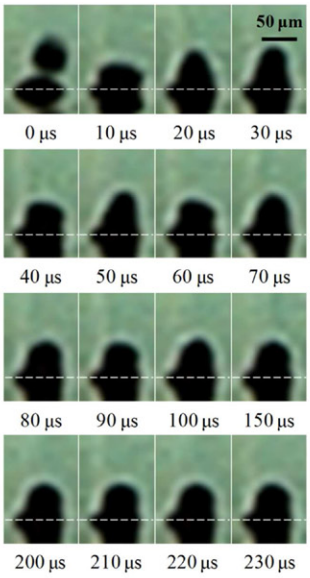

(a)

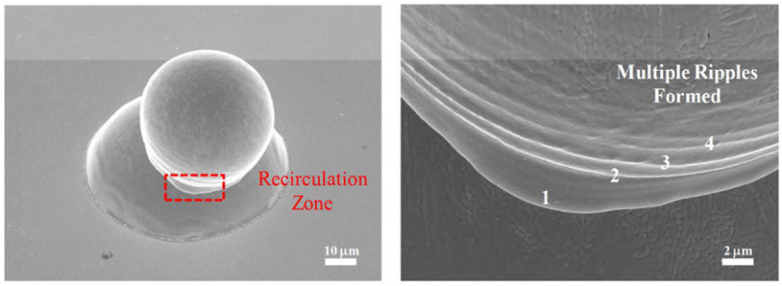

(b)

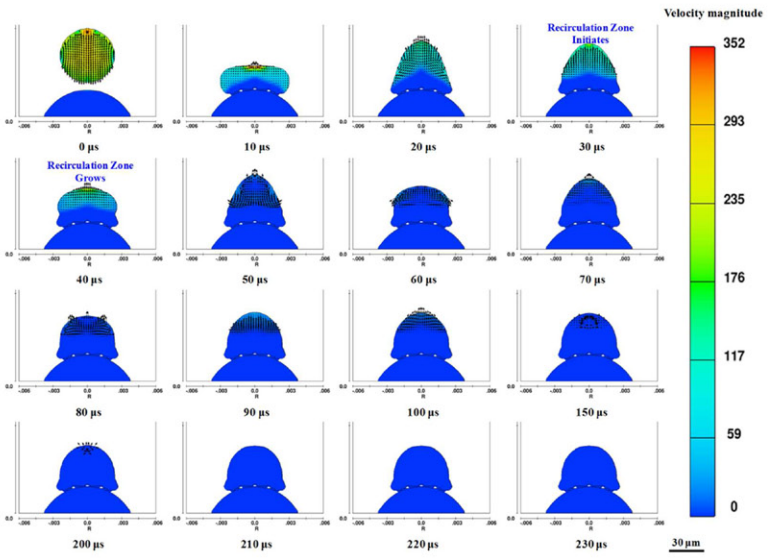

(c)

Figure 7. (a) Evolution of the droplet impact and solder pile up process for the experimental observations with condition B in table 1. The distance from the jet nozzle to the substrate is 0.5 mm. The dashed lines demarcate the line of droplet impact on the substrate, which separated the outline of the droplet from that of its reflection on the substrate. (b) Morphology of droplet impact on a gold-plated glass substrate surface, with four ripples having formed. (c) 2D images of the velocity magnitude of the pileup droplet by streamlines, as obtained from the numerical simulations.

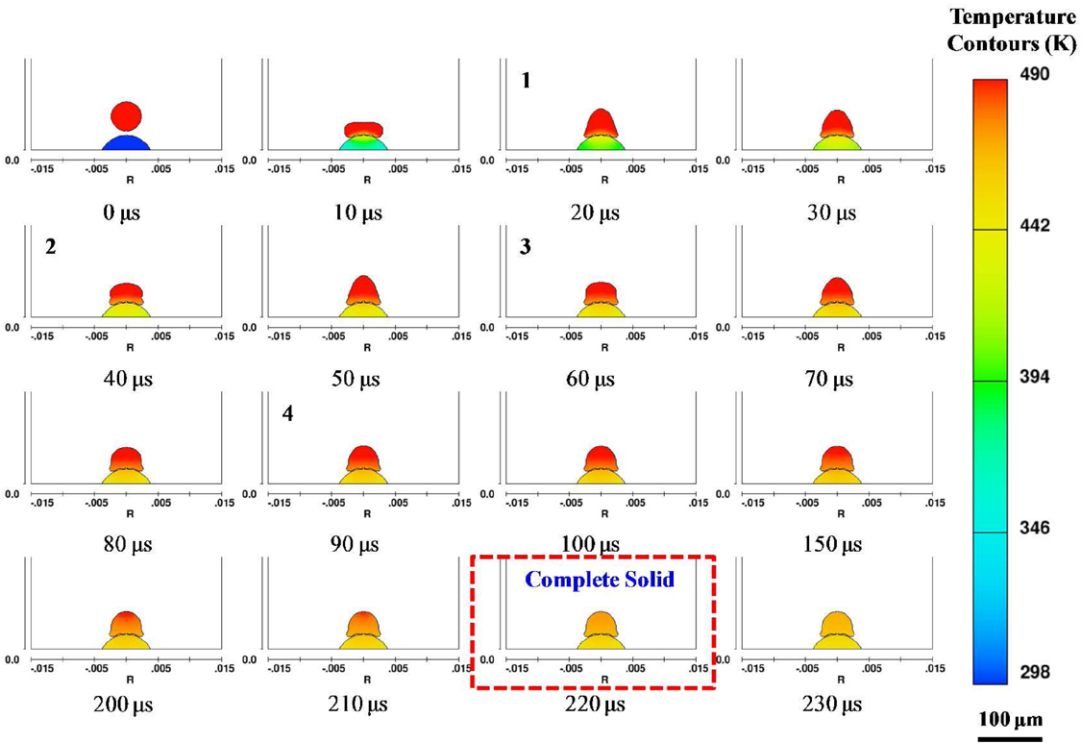

(a)

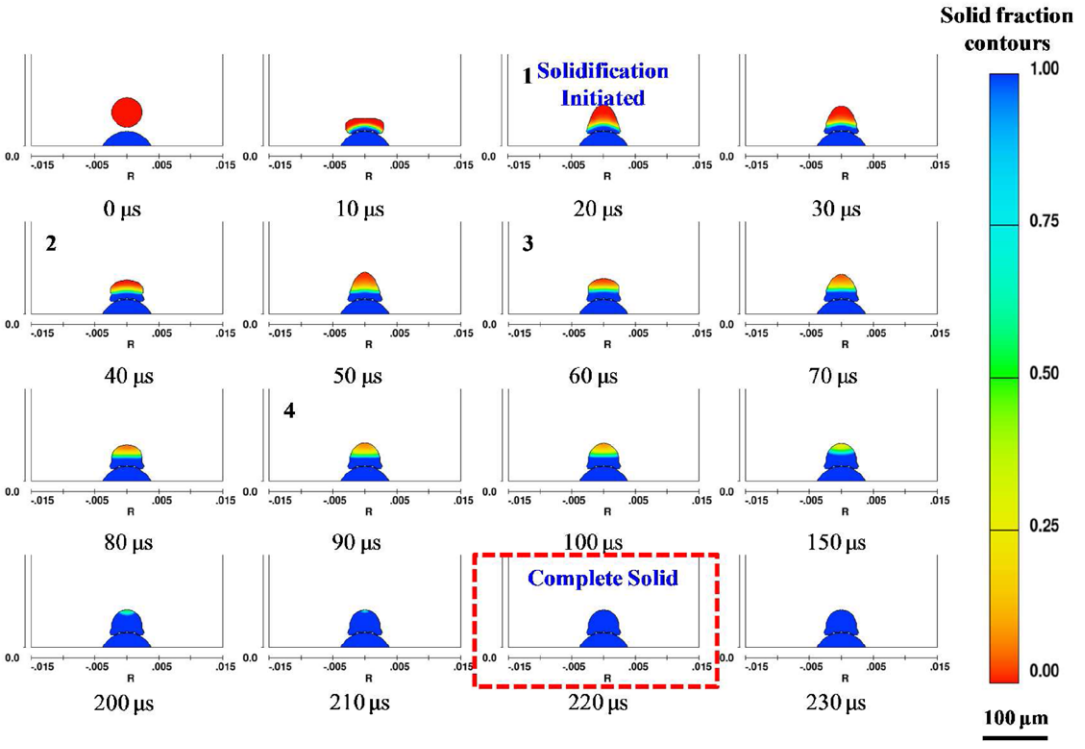

(b)

Figure 8. (a) Calculated 2D images of the temperature contour of the pileup droplet. (b) Simulated deformation and solid fraction of a 48 μm diameter Sn–3Ag–0.5Cu solder droplet on the gold-plated substrate at 490 K with an impact velocity of 3.5 m s^{-1}. The numeral represents the number of times that recoil occurred.

motion is completely damped at 220 μs. Figure 7(b) shows an SEM image of one droplet piling up on another. Attinger *et al* [1] investigated the molten microdroplet surface deposition and solidification transient behavior and wetting angle dynamics. They found that the ripples on the solidified drop surface are due to a strong coupling between flow oscillations and solidification. These results showed that there are four ripples formed, with the first ripple on the bottom of the droplet.

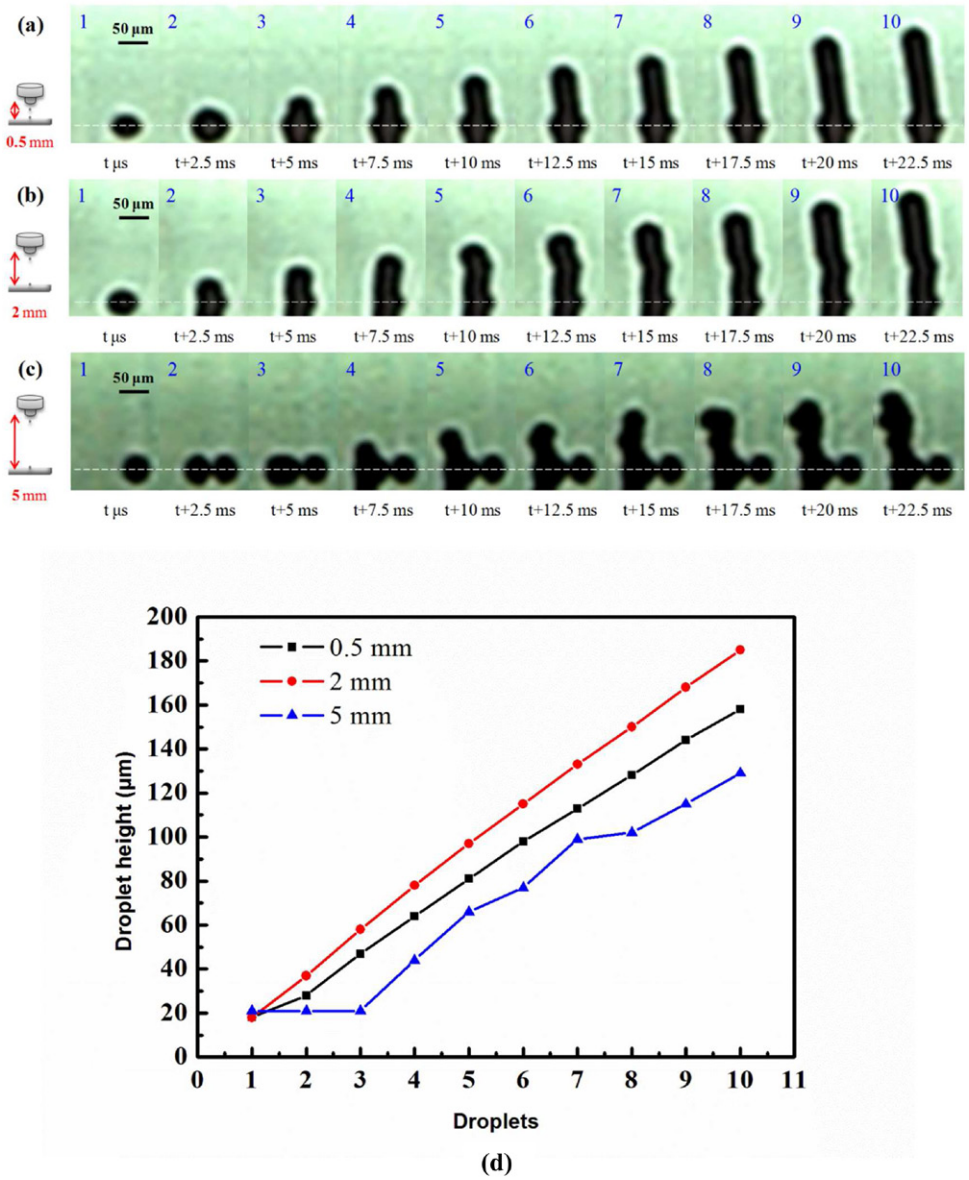

Figure 9. Impact of molten solder droplet on a gold-plated substrate surface at a temperature of 300 K with a diameter $D_0 = 37$ μm, impact velocity of 2.0 m s^{-1}, Reynolds number Re = 269.6, Weber number We = 2.2, Ohnesorge number Oh = 5.4 × 10^{-3}, and the distance from the jet nozzle to substrate is (a) 0.5 mm, (b) 2 mm, (c) 5 mm, the dashed lines demarcate the line of droplet impact on the substrate, which separated the outline of the droplet from that of its reflection on the substrate. (d) The height of various droplets ejected with the pile up corresponding to condition A in table 1.

Figure 7(c) shows 2D images of the velocity magnitude of the pileup droplet by streamlines, as obtained from the numerical simulations. The recirculation zone initiates and then maintains the first droplet at 30 μs while it moves upward. As the front propagates, the recirculation zone grows in various stages of oscillation at 40 μs. The velocity field apparently decreases when the time increases from 0 μs to 210 μs. Waldvogel *et al* [33] investigated the solidification phenomena in picoliter size solder droplet deposition on a composite substrate. The results of their simulations showed the behavior of the recirculation zone (solder) at temperatures above 200 °C from 43.3 μs to 50.8 μs were observed. Their numerical results show good agreement with our research.

Figure 8(a) shows 2D images of the temperature contour of the pileup droplet impact on the solidified droplet. The second (molten) droplet impinges the top surface of a solidified droplet. At 10 μs, it is clear that the heat transfers from the molten solder to the solidified droplet, which would cause remelting of the solidified droplet. It is possible that the spreading of the droplet is driven by the impact velocity. At 20 μs, the second droplet is caused the first recoil on the top surface of solidified droplet. During 20–220 μs, the temperature of second droplet was decreased due to the heat transfer to the solidified droplet. Figure 8(b) shows the simulated deformation and solid fraction of a 48 μm diameter Sn–3Ag–0.5Cu solder droplet on top of a solidified droplet at 490 K with an impact velocity of 3.5 m s^{-1}. The results show that the initial solidification of the second (molten) droplet is started at 20 μs, then the second droplet changed to a complete solid at 220 μs. The numerical simulation and experimental observations of pile

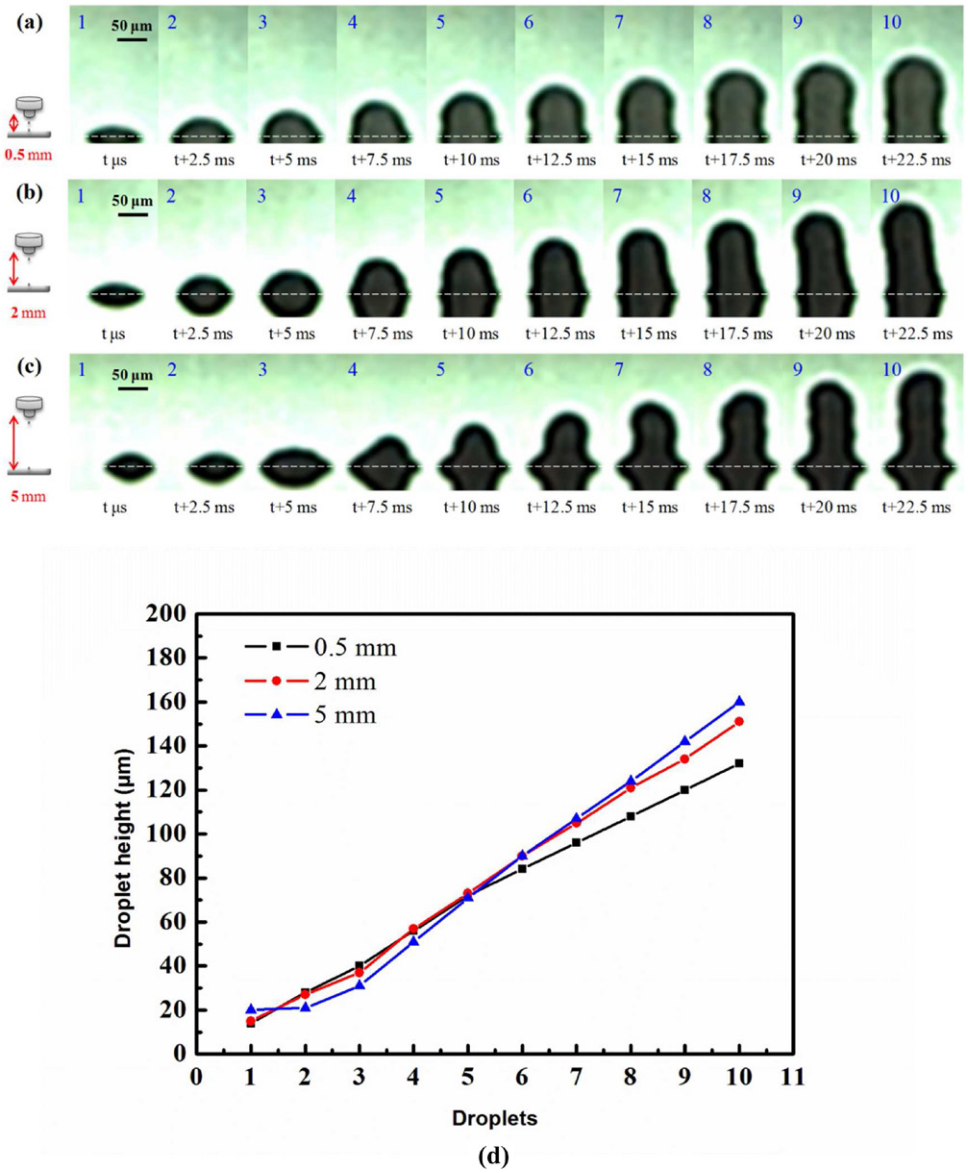

Figure 10. Impact of molten solder droplet on a gold-plated substrate surface at a temperature 300 K with a diameter of $D_0 = 65$ μm, impact velocity of 3.7 m s^{-1}, Reynolds number Re = 1010.1, Weber number We = 15.1, Ohnesorge number Oh = 3.8 × 10^{-3}, and the distance from the jet nozzle to substrate is (a) 0.5 mm, (b) 2 mm, (c) 5 mm, the dashed lines demarcate the line of droplet impact on the substrate, which separated the outline of the droplet from that of its reflection on the substrate. (d) The height of various droplets ejected with the pile up corresponding to condition C in table 1.

up show significant deformation prior to the onset of solidification below the second droplet at 20 μs. However, the numerical simulation shows that the post-spreading oscillations and the solidification phase occur together from 20 μs to 220 μs. The oscillations were observed to solidify after about four ripples. Finally, the complete solid was observed and the shape appears to be a liquid column at 220 μs. As the fluid continues to recoil and subsequently oscillate, the droplet freezes the deforming droplet in various stages of oscillation [33]. These results show that details of the process of droplet impact and solder pile up can be obtained from the numerical simulations, including those related to impacting, spreading, post-spreading oscillations and solidification. In addition, the numerical simulations by validated with the results of the experiments.

3.2. Effects of jet height and pulse voltage on droplet pile up

To better understand the pile up quality mechanism, we further jetted solder droplets to form a column with different pulse voltages and jet heights of 0.5, 2, and 5 mm.

Figure 9 shows the impact of molten solder droplets on a gold-plated substrate surface with different distances from the jet nozzle to substrate (condition A), and with a diameter $D_0 = 37$ μm, pulse voltage $V_2 = -45$ V (an impact velocity of 2.0 m s^{-1}), Reynolds number Re = 269.6, Weber number We = 2.2, Ohnesorge number Oh = 5.4 × 10^{-3}. The series of droplet pile up processes shown in figure 9(a) reveal a correlated arrangement of 0.5 mm on the gold-plated substrate surface. The results indicate that the column was caused by regular and stable pile up on the sample. Figure 9(b) shows

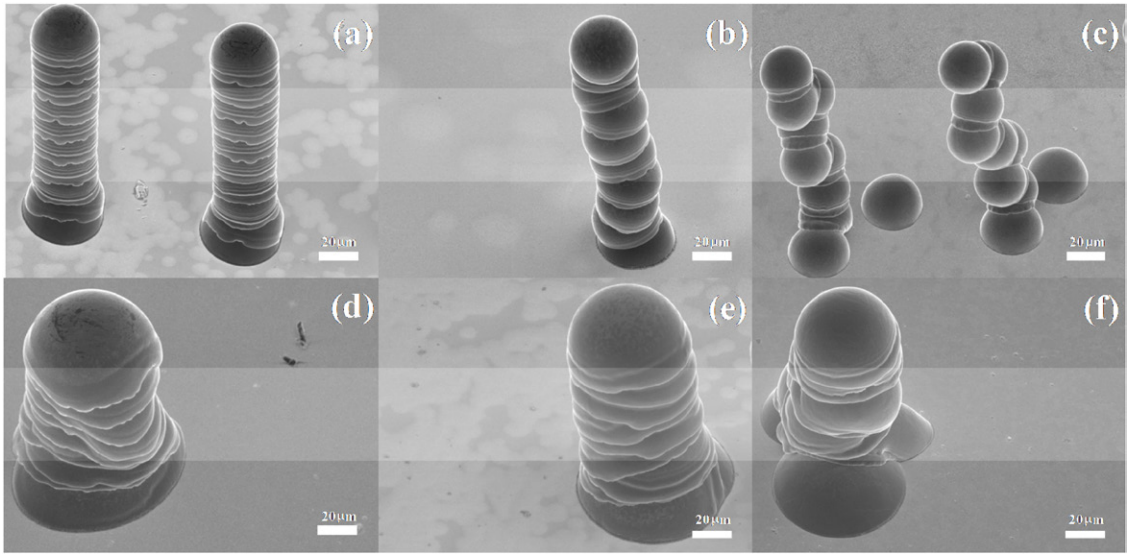

Figure 11. The SEM images of the pile up shapes of solder droplets when the pulse voltage is controlled and there are various jet heights. (a) Neat $V_2 = -45$ V, 0.5 mm; (b) $V_2 = -45$ V, 2.0 mm; (c) $V_2 = -45$ V, 5.0 mm; (d) neat $V_2 = -55$ V, 0.5 mm; (e) $V_2 = -55$ V, 2.0 mm; (f) $V_2 = -55$ V, 5.0 mm.

Table 3. Comparison of pulse voltage conditions based on the results of the experiment and Weber's predictions.

V_2 pulse voltage (V)	Impact velocity (m s^{-1})	Volume (pl)	We	Re	Oh
−45	2.0	25	2.2	269.6	3.8×10^{-3}
−50	3.5	56	9.0	627.0	4.8×10^{-3}
−55	3.7	144	15.1	1010.1	5.4×10^{-3}

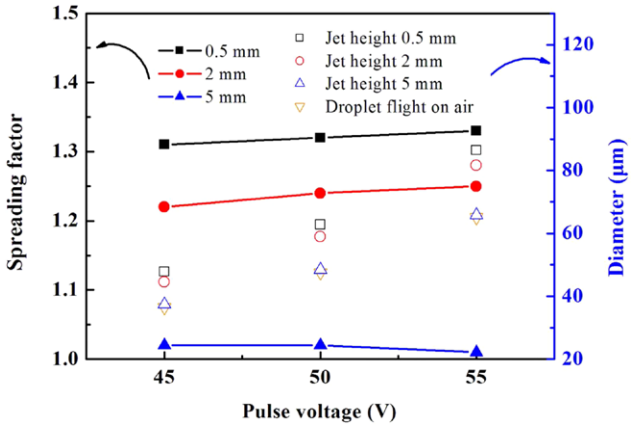

Figure 12. The effects of the pulse voltage on a gold-plated substrate with different spacings. ■: The distance from the nozzle to substrate is 0.5 mm, ●: The distance from the nozzle to substrate is 2 mm, and ▲: The distance from the nozzle to substrate is 5 mm.

the results of the droplet pile up on the substrate with a pulse voltage of $V_2 = -45$ V and jet height of 2 mm. It is clear that there was a rather strong disagreement between the column of droplet pile up and substrate. Figure 9(c) shows the droplet pile up on the substrate with a pulse voltage of $V_2 = -45$ V and jet height of 5 mm, and it can be seen that there was an irregular pile up on the substrate. Figure 9(d) shows the heights of various droplets ejected with the pile up corresponding to condition A in table 1. The results show that the pile up of the droplet column was increased steadily when the jet height was increased below 5 mm.

Figure 10 shows the impact of molten solder droplets on the gold-plated substrate surface at different distances from a jet nozzle (condition C), with a diameter of $D_0 = 65$ μm, pulse voltage $V_2 = -55$ V (an impact velocity of 3.7 m s^{-1}), Reynolds number Re = 1010.1, Weber number We = 15.1, and Ohnesorge number Oh = 3.8×10^{-3}. Figure 10(a) shows the droplet pile up on a gold-plated substrate with a pulse voltage of $V_2 = -55$ V and jet height of 0.5 mm, as obtained with a high-speed digital camera system. The results show that the liquid column of the droplet pile up was vertical in relation to the substrate. Figure 10(b) shows the droplet pile up on the substrate with a pulse voltage of $V_2 = -55$ V and jet height of 2 mm. It can be seen that the column of the droplet pile up was similar to a tile. Figure 10(c) shows the droplet pile up on a gold-plated substrate with a pulse voltage of $V_2 = -55$ V and jet height of 5 mm. At the beginning three droplets impacted in different positions, and then a column formed an irregular pile up on the sample. Figure 10(d) shows the heights of various droplets ejected with the pile up corresponding to condition C in table 1. The results show that the pile up of the droplet column was formed as the jet height increased.

The SEM results help us to confirm the pile up shape distribution of these droplets, especially for the column shown in figure 10. Based on all the pile up quality and accuracy obtained in this work, we suggest the following scenario to explain the successful pile up of the solder droplets by using the inkjet printing process. Figures 11(a) and (d) show neat pile up when the jet height was 0.5 mm. A comparison of pulse

voltage conditions based on the results of the experiment and Weber's predictions is shown in table 3. It is thus possible that the stability and accuracy of the droplets were enhanced as the Weber number decreased from 15.1 to 2.2 [18]. It follows from this that when the jet height was more than 2 mm, the accuracy of the droplet pile up decreased. This seems to be because the initial conditions (orientation of the velocity vector of the droplet when it detaches from the nozzle) will be amplified more (lead to greater lateral displacements) the longer the droplet trajectory.

3.3. Effects of spread factor on droplet behavior

Figure 12 presents the effects of the pulse voltage on a gold-plated substrate with different spacings. The results of the experiment show that the single droplet formation was achieved by increasing the V_2 voltage to between 45 V and 55 V, and the resulting droplet sizes of the pre-impact phase in air were 37 μm, 48 μm, and 65 μm. When the jet height increased from 0.5 to 5 mm the spreading factor was decreased from 1.3 to 1.0. It can thus be seen that the spreading factor decreased as the jet height increased from 0.5 mm to 5 mm during the inkjet printing process. However, the spreading factor of the droplet did not change when the pulse voltage was increased.

4. Conclusion

This paper carried out a predominantly experimental investigation of the transport processes associated with molten solder droplets impacting and solidifying onto a gold-plated substrate in air. The behaviors of molten droplets have been determined and presented as a function of the impact velocity for various combinations of the pulse voltage and the jet height parameters. The following conclusions can be drawn based on the results of this study.

1. With regard to the experimental and simulated impact of droplets, the pile up of two droplets contributed to the spreading and deformation of a droplet on the substrate. Details of the pile up behavior can be thus be obtained, including the complex post-spreading oscillations and solidification that occur together.
2. The pile up of the droplets is located in the recirculation zone, and the number of ripples that forms is four.
3. The optimum conditions of the metallic micro structure with respect to the value of the jet height (0.5 mm) and the impact velocity (3.7 m s^{-1}) have been successfully obtained. The quality and accuracy of a printed droplet pile up can be evaluated using the Reynolds number or the Weber number.
4. The spreading factor seems to be more influenced from 1.33 to 1.01 by the jet height (0.5 mm–5 mm) of the solder droplet compared to the different inkjet printing conditions on the substrate.

Acknowledgments

This study was supported by the Research Center for Energy Technology and Strategy (RCETS), National Cheng Kung University in Taiwan, which is gratefully acknowledged. A part of the present work was also supported by the Ministry of Science and Technology (MOST 103-2221-E-006-059-MY3) and the Additive Manufacturing Innovation Department, Industrial Technology Research Institute (ITRI) Southern Region Campus in Taiwan.

References

[1] Attinger D, Zhao Z and Poulikakos D 2000 Experimental study of molten microdroplet surface deposition and solidification: transient behavior and wetting angle dynamics *Trans. ASME, J. Heat Transfer* **122** 544–56
[2] Pasandideh-Fard M, Chandra S and Mostaghimi J 2002 A three-dimensional model of droplet impact and solidification *Int. J. Heat Mass Transf.* **45** 2229–42
[3] Haferl S and Poulikakos D 2003 Experimental investigation of the transient impact fluid dynamics and solidification of a molten microdroplet pile-up *Int. J. Heat Mass Transfer* **46** 535–50
[4] Le Bot C, Vincent S and Arquis E 2005 Impact and solidification of indium droplets on a cold substrate *Int. J. Therm. Sci.* **44** 219–33
[5] Yarin A L 2006 Drop impact dynamics: splashing spreading receding bouncing *Annu. Rev. Fluid Mech.* **38** 159–92
[6] Vincent S, Le Bot C, Sarret F, Meillot E, Caltagirone J P and Bianchi L 2015 Penalty and Eulerian-Lagrangian VOF methods for impact and solidification of metal droplets plasma spray process *Comput. Fluids* **113** 32–41
[7] Yang H A, Wu M C and Fang W L 2005 Localized induction heating solder bonding for wafer level MEMS packaging *J. Micromech. Microeng.* **15** 394–9
[8] Esashi M 2008 Wafer level packaging of MEMS *J. Micromech. Microeng.* **18** 073001
[9] Wallace D, Hayes D, Chen T, Shah V, Radulescu D, Cooley P, Wachtler K and Nallani A 2004 Think additive: ink-jet deposition of materials for MEMS packaging *6th Topical Workshop on Packaging of MEMS and Related Micro-Nano-Bio Integrated Systems Volume: IMAPS MEMS (2004)* pp 1–7
[10] Hayes D J, Grove M E and Cox W R 1999 Development and application by ink-jet printing of advanced packaging materials *Proc. of Int. Symp. on Advanced Packaging Materials: Processes, Properties and Interfaces* pp 88–93
[11] Liu Q and Orme M 2001 High precision solder droplet printing technology and the state-of-the-art *J. Mater. Process. Technol.* **115** 271–83
[12] Kloeser J, Coskina P, Aschenbrenner R and Reichl H 2002 Bump formation for flip chip and CSP by solder paste printing *Microelectron. Reliab.* **42** 391–8
[13] Tsai M H, Hwang W S and Chou H H 2009 The micro-droplet behavior of a molten lead-free solder in an inkjet printing process *J. Micromech. Microeng.* **19** 125021
[14] Son H Y, Nah J W and Paik K W 2005 Formation of Pb/63Sn solder bumps using a solder droplet jetting method *IEEE Trans. Electron. Packag. Manuf.* **28** 274–81
[15] Tian D W, Wang C Q and Tian Y H 2008 Effect of solidification on solder bump formation in solder jet process: simulation and experiment *Trans. Nonferr. Met. Soc. China* **18** 1201–8

[16] Attinger D and Poulikakos D 2001 Melting and resolidification of a substrate caused by molten microdroplet impact *Trans. ASME, J. Heat Transfer* **123** 1110–22
[17] Schiaffino S and Sonin A A 1997 Molten droplet deposition and solidification at low Weber numbers *Phys. Fluids* **9** 3172–87
[18] Van Dam D B and Le Clerc C 2004 Experimental study of the impact of an ink-jet printed droplet on a solid substrate *Phys. Fluids* **16** 3403–14
[19] Haferl S and Poulikakos D 2002 Transport and solidification phenomena in molten microdroplet pileup *J. Appl. Phys.* **92** 1675–89
[20] Li H J, Wang P Y, Qi L H, Zuo H S, Zhong S Y and Hou X H 2012 3D numerical simulation of successive deposition of uniform molten Al droplets on a moving substrate and experimental validation *Comput. Mater. Sci.* **65** 291–301
[21] Chao Y P, Qi L H, Zuo H S, Luo J, Hou X H and Li H J 2013 Remelting and bonding of deposited aluminum alloy droplets under different droplet and substrate temperatures in metal droplet deposition manufacture *Int. J. Mach. Tools Manuf.* **69** 38–47
[22] Zuo H S, Li H J, Qi L H, Luo J, Zhong S Y and Wu Y F 2015 Effect of non-isothermal deposition on surface morphology and microstructure of uniform molten aluminum alloy droplets applied to three-dimensional printing *Appl. Phys.* A **118** 327–35
[23] Shin D Y, Grassia P and Derby B 2004 Numerical and experimental comparisons of mass transport rate in a piezoelectric drop-on-demand inkjet print head *Int. J. Mech. Sci.* **46** 181–99
[24] Haferl S, Butty V, Poulikakos D, Giannakouros J, Boomsma K, Megaridis C M and Nayagam V 2001 Freezing dynamics of molten solder droplets impacting onto flat substrates in reduced gravity *Int. J. Heat Mass Transfer* **44** 3513–28
[25] Gong S C 2005 Spreading of droplets impacting on smooth solid surface *Japan. J. Appl. Phys.* **44** 3323–4
[26] Li R, Ashgriz N and Chandra S 2010 Maximum spread of droplet on solid surface: low Reynolds and Weber numbers *Int. J. Therm. Sci.* **132** 061302
[27] Luo J L, Qi L H, Zhong S Y, Zhou J M and Li H J 2012 Printing solder droplets for micro devices packages using pneumatic drop-on-demand (DOD) technique *J. Mater. Process. Technol.* **212** 2066–73
[28] Wu J, Wei Z Y, Chen Z, Li S L and Tang Y P 2014 Numerical investigation of pile up process in metal microdroplet deposition manufacture *Micromachines* **5** 1429–44
[29] Hirt C W and Nichols B D 1981 Volume of fluid (VOF) method for the dynamics of free boundaries *J. Comput. Phys.* **39** 201–25
[30] Glazer J 1994 Microstructure and mechanical properties of Pb-free solder alloys for low-cost electronic assembly: a review *J. Electron. Mater.* **23** 693–700
[31] Mundo C, Sommerfeld M and Tropea C 1995 Droplet-wall collisions: experimental studies of the deformation and breakup process *Int. J. Multiph. Flow* **21** 151–73
[32] Thoroddsen S T and Sakakibara J 1998 Evolution of the fingering pattern of an impacting drop *Phys. Fluids* **10** 1359–74
[33] Waldvogel J M and Poulikakos D 1997 Solidification phenomena in picoliter size solder droplet deposition on a composite substrate *Int. J. Heat Mass Transfer* **40** 295–309